# Pressure and folding effects on the buckling of a freestanding compressed thin film

J. Durinck[1,*] S. Hamade[2] J. Grilhé[1] and J. Colin[1]

[1]*Institut Pprime, UPR 3346 CNRS, Université de Poitiers-ENSMA-CNRS, 86073 Poitiers cedex, France*

[2]*Polytech'Lab, UPR UCA 7498, Université Nice Sophia Antipolis, 06903 Sophia Antipolis cedex, France*

(Received 25 January 2023; accepted 2 March 2023; published 20 March 2023)

The combined effects of compressive stress, applied pressure, and edge folding of a freestanding thin film have been theoretically investigated on the buckle morphologies of the structure. In the framework of the Föppl–von Kármán theory of thin plates, the different buckle profiles have been analytically determined, and two buckling regimes have been identified for the film: one regime where the transition from upward to downward buckling is continuous, and one that is discontinuous (snap-through). The critical pressures characterizing the different regimes have then been determined, and an hysteresis cycle has been identified through the study of buckling versus pressure. The case in which the thin film is deposited on a substrate has also been discussed.

DOI: 10.1103/PhysRevE.107.035003

## I. INTRODUCTION

A large number of microsystems of various shapes and materials are currently manufactured with the aim of accessing different functionalities, ranging from mechanical to electronic functionalities, including chemical and optical ones. In a large number of applications in the engineering field, the microfabricated devices are composed of slender structures whose mechanical behavior must be understood and controlled. It is now widely acknowledged that structures under strain can undergo mechanical instabilities when geometrical nonlinearities are considered. This corresponds to film buckling, multilayered structures wrinkling, and layer folding [1–7]. Significant efforts have therefore been made to characterize the threshold of these instabilities in terms of buckling pattern, shape, and critical load [8–14] in order to control the mechanical behavior of the recently elaborated metamaterials [15–19]. For example, a numerical energy-based method has been developed to analyze the condition for manufacturing freestanding films when pre- and postbuckling conditions apply [20]. Likewise, the elastic snap-through phenomenon that has been identified for structures under various conditions, such as mechanical loads [21] or capillarity forces [22,23], has been used to control the viscous flow in a channel by means of an elastic arch [24].

In the field of materials science and metallurgy, it is also well-established that an internal compressive stress [25,26] in the films can be the cause, when it exceeds a critical value, of interface delamination and thin-film buckling leading to various patterns such as circular blisters, straight-sided buckles, and wormlike wrinkles (see [13,14,27–35] and references therein). The problem of blister folding has also been investigated, and the configurational stability of the buckled patterns has been characterized [36]. Later, the folding of buckles in the case of $Y_2O_3$ and Au thin films deposited on Si substrates was studied considering that the top side or the circumference of the buckles undergoes a plastic folding [37–39]. This folding can be described in terms of low-angle tilt boundaries modeled using vertical rows of edge dislocations [40]. For Al thin films deposited on rigid substrates, molecular-dynamics simulations at finite temperature have therefore been carried out, and the role of grain boundaries in the plasticity mechanisms leading to film folding have been identified [41].

The effect of pressure has also been considered, and the pressure-induced redeposition of the buckled film has been characterized [42]. More recently, the combined effects of plastic folding and atmospheric pressure have been considered through finite-element simulations [43]. The formation of donut- and croissant-like patterns has thus been explained when the films are deposited on a substrate. Likewise, the pressure on the free-surface of Ta thin films deposited on a Si substrate has been found to be responsible for the shape transition from circular blisters to ring-shaped buckles, when blister diameters reach a critical value [44].

From the previously cited literature, it thus appears that the study of the combined effects of pressure and folding due to plasticity on the mechanical behavior of metallic layered materials is a topic of research that deserves attention. It is the purpose of the present work to investigate the combined effect of an applied pressure and edge folding in the case of a clamped free-standing thin film under compressive stress. The possibility of upward and downward buckling has then been discussed as a function of the pressure and folding angle. The configuration where the film is also deposited on a substrate has been discussed.

## II. MODELING OF THE BUCKLING PROBLEM AND GOVERNING EQUATIONS

An initially planar thin film of thickness $h$, Young's modulus $E$, and Poisson's ratio $\nu$ is submitted to in-plane compressive stress $\sigma^0_{xx} = \sigma^0_{yy} = -\sigma_0$, with $\sigma_0 > 0$ [see Fig. 1(a) for axes]. It is assumed that each of the two rigid parts of the film is lying on a semi-infinite substrate assumed to be infinitely stiff, the freestanding part being of length

*julien.durinck@univ-poitiers.fr

 

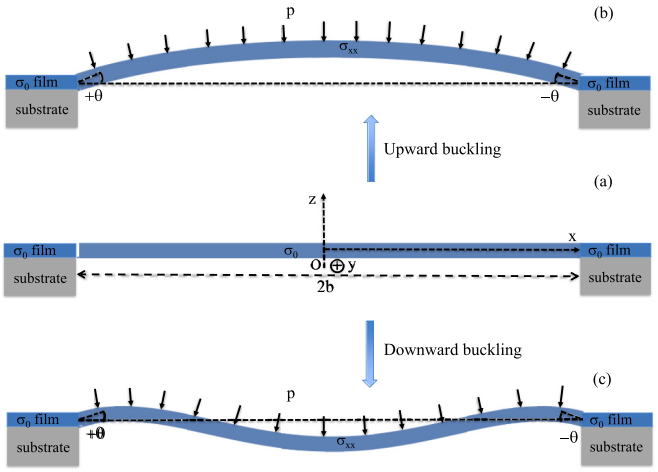


FIG. 1. (Sketch not to scale) Thin film of thickness $h$ deposited on a semi-infinite substrate submitted to an in-plane stress $\sigma_{xx}^0 = \sigma_{yy}^0 = -\sigma_0$. The free-standing part of the film of length $2b$ is submitted to an external applied pressure $p$. (a) Planar configuration. (b) Upward buckling of the free-standing film when the pressure is smaller than a critical value $\tilde{p}_c$. (c) Downward buckling when $\tilde{p} > \tilde{p}_c$.

$2b$, with $h/b \ll 1$. The case in which the film is deposited on a continuous substrate and delaminated on a $2b$ length will be discussed later. Depending on $\sigma_0$ values, the infinitely long freestanding film in the $(Oy)$ direction may buckle in the $(Oxz)$ plane [13]. It is thus considered that, once buckled, the freestanding part of the film undergoes an applied overpressure $p$ on its upper free-surface corresponding to the mismatch between the pressures applied on its upper and lower free-surfaces. In the following, the cases of buckling in the upward direction in Fig. 1(b) or in the downward direction in Fig. 1(c) are considered, assuming that, due to plastic deformation, both extremities of the film are folded, in the upper part of the $(Oxz)$ plane, of an angle $\{\mp\theta, \theta > 0\}$ with respect to the horizontal axes [13]. It is emphasized at this point that the study of the plasticity mechanisms at the microscopic scale responsible for this folding effect including defects such as dislocations and/or grain boundaries is beyond the scope of the present analysis [36–39,43,44]. Consequently, the values of the folding angle $\theta$ will be arbitrarily chosen in the following. Considering the plane strain hypothesis of the isotropic elasticity theory [45], the two components of the elastic displacements, only depending on $x$ variable and labeled $u$ and $w$ along the $(Ox)$ and $(Oy)$ axes, respectively, satisfy in the framework of the Föppl–von Kármán (FvK) theory of thin plates [13] the following set of equations:

$$\frac{d^4w}{dx^4} - \frac{h}{D}\sigma_{xx}\frac{d^2w}{\partial x^2} = \frac{p}{D}, \tag{1}$$

$$u(\pm b) = 0, \tag{2}$$

$$w(\pm b) = 0, \tag{3}$$

$$\left(\frac{dw}{dx}\right)_{x=\pm 1} = \mp \tan\theta, \tag{4}$$

to which the strain-stress relation

$$\frac{1-\nu^2}{E}(\sigma_0 + \sigma_{xx}) = \frac{du}{dx} + \frac{1}{2}\left(\frac{dw}{dx}\right)^2 \tag{5}$$

must be added, with $\sigma_{xx}$ the constant stress in the buckled film and $D = Eh^3/[12(1-\nu^2)]$. Introducing the dimensionless parameters and variables $\tilde{h} = h/b$, $\tilde{\sigma}_{xx} = \frac{1-\nu^2}{E}\sigma_{xx}$, $\tilde{\sigma}_0 = \frac{1-\nu^2}{E}\sigma_0$, $\tilde{p} = \frac{1-\nu^2}{E}p$, $\alpha^2 = -\frac{12}{\tilde{h}^2}\tilde{\sigma}_{xx}$, $\alpha_0^2 = \frac{12}{\tilde{h}^2}\tilde{\sigma}_0$, $\tilde{x} = x/b$, $\tilde{u} = u/b$, and $\tilde{w} = w/b$, the system of Eqs. (1)–(5) has been recast as

$$\frac{d^4\tilde{w}}{d\tilde{x}^4} + \alpha^2\frac{d^2\tilde{w}}{\partial\tilde{x}^2} = \frac{12}{\tilde{h}^3}\tilde{p}, \tag{6}$$

$$\tilde{u}(\pm 1) = 0, \tag{7}$$

$$\tilde{w}(\pm 1) = 0, \tag{8}$$

$$\left(\frac{d\tilde{w}}{d\tilde{x}}\right)_{\tilde{x}=\pm 1} = \mp \tan\theta, \tag{9}$$

$$\frac{\tilde{h}^2}{12}(\alpha_0^2 - \alpha^2) = \frac{d\tilde{u}}{d\tilde{x}} + \frac{1}{2}\left(\frac{d\tilde{w}}{d\tilde{x}}\right)^2. \tag{10}$$

Solving this system of Eqs. (6)–(9), and integrating Eq. (10) on the interval $\tilde{x} \in [-1, +1]$, leads to the following elastic solution:

$$\begin{aligned}\tilde{w}(\tilde{x}) = \frac{1}{\alpha^3\tilde{h}^3}\{&6\alpha\tilde{p}(\tilde{x}^2 - 1)\\ &+ (\alpha^2\tilde{h}^3\tan\theta + 12\tilde{p})\\ &\times(\cos\alpha\tilde{x} - \cos\alpha)\sin^{-1}\alpha\},\end{aligned} \tag{11}$$

$$\begin{aligned}\tilde{u}(\tilde{x}) = \frac{\tilde{h}^2}{12}(\alpha_0^2 - \alpha^2)\tilde{x} - \frac{1}{8\alpha^6\tilde{h}^6}\{&192\alpha^2\tilde{p}^2\tilde{x}^3\\ &+ (\alpha^2\tilde{h}^3\tan\theta + 12\tilde{p})\sin^{-1}\alpha[96\alpha\tilde{p}\tilde{x}\cos\alpha\tilde{x}\\ &- 96\tilde{p}\sin\alpha\tilde{x} + \alpha(\alpha^2\tilde{h}^3\tan\theta + 12\tilde{p})\sin^{-1}\alpha\\ &\times(2\alpha\tilde{x} - \sin 2\alpha\tilde{x})]\}.\end{aligned} \tag{12}$$

The parameter $\alpha$ related to the stress in the film, once it is buckled, is implicitly determined by Eq. (10) recast as

$$\begin{aligned}\frac{\tilde{h}^2}{12}(\alpha_0^2 - \alpha^2) - \frac{1}{4\alpha^6\tilde{h}^6}\{&-48\tilde{p}(\alpha^2(\tilde{h}^3\tan\theta - 2\tilde{p})\\ &+12\tilde{p}) + \alpha(\alpha^2\tilde{h}^3\tan\theta + 12\tilde{p})[(36\tilde{p} - \alpha^2\tilde{h}^3\tan\theta)\\ &\times\tan^{-1}\alpha + \alpha(\alpha^2\tilde{h}^3\tan\theta + 12\tilde{p})\sin^{-2}\alpha]\} = 0,\end{aligned} \tag{13}$$

the smallest absolute value of $\alpha$ being the one selected, since it corresponds to the more relaxed configuration. It has to be noted that, because of the imposed angle $\pm\theta$ at the extremities of the film, the relaxed buckle configuration can be found to be either in compression ($\tilde{\sigma}_{xx} < 0$ and $\alpha^2 > 0$) or in tension ($\tilde{\sigma}_{xx} > 0$ and $\alpha^2 < 0$). Thus, solutions have to be sought for $\alpha \in$ Re in compression and for $\alpha \in$ Im in tension.

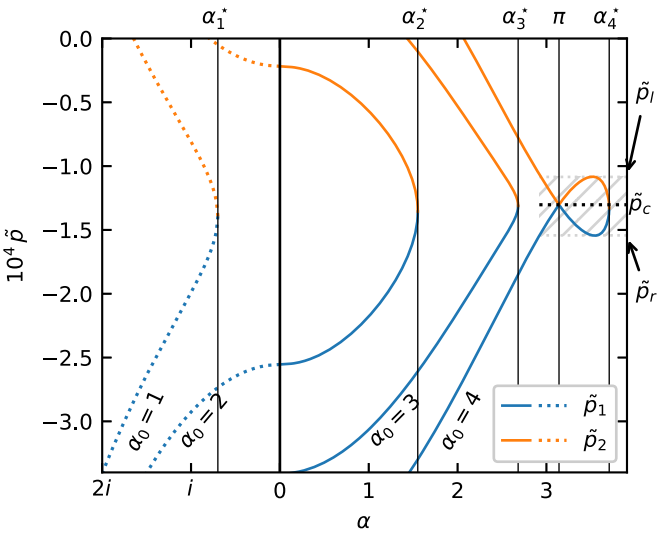


FIG. 2. Evolution of pressures $\tilde{p}_1$ and $\tilde{p}_2$ with respect to $\alpha$ for different values $\alpha_0 = 1$, 2, 3, and 4 and for $\theta = \pi/20$ and $\tilde{h} = 0.1$. The pressures corresponding to buckle configurations in tension (compression) are shown by dotted lines (solid lines).

From Eq. (11), the buckle profile parameter $\tilde{\delta} = \tilde{w}(0)$ defined as

$$\tilde{\delta} = \frac{-6\alpha\tilde{p} + (\alpha^2\tilde{h}^3\tan\theta + 12\tilde{p})\tan\frac{\alpha}{2}}{\alpha^3\tilde{h}^3} \tag{14}$$

has also been considered in the following to characterize the thin-film morphology.

## III. FREESTANDING FILM BUCKLING

### A. Buckled configurations with respect to pressure

Although we could not obtain an explicit analytical solution for $\alpha$ versus pressure from Eq. (13), an analytical expression of the pressure versus $\alpha$ can be provided. More specifically, two solutions labeled $\tilde{p}_1$ and $\tilde{p}_2$ (with $\tilde{p}_1 < \tilde{p}_2 < 0$) have been explicitly derived from Eq. (13), but their expressions have not been displayed in this paper for the sake of simplicity. The pressures $\tilde{p}_1$ and $\tilde{p}_2$ have been plotted in Fig. 2 with respect to $\alpha$ for $\alpha_0 = 1$, 2, 3, and 4. It is seen that, for $\alpha_0 = 1$, the solutions correspond to buckled configurations in tension ($\alpha^2 < 0$) for any pressure. For the other considered values of $\alpha_0$ (2, 3, and 4), the solutions can correspond to either buckled configurations in tension or in compression, depending on the value of the pressure. Another result highlighted by Fig. 2 is that for $\alpha_0 = 1$, 2, and 3, one pressure value corresponds only to one buckled configuration, i.e., one value of $\alpha$. On the contrary, for $\alpha_0 = 4$, when $\tilde{p}_1$ and $\tilde{p}_2$ take values in the range $[\tilde{p}_l, \tilde{p}_r]$, three different buckled configurations can be found, underlining a possible snap-through between two stable configurations (the third one being unstable). Before studying the stability of the configurations, which is required to fully understand the snap-through, the critical value $\alpha_{0c}$ at which the system transits from a stable behavior ($\alpha_0 < \alpha_{0c}$) to an unstable one ($\alpha_0 > \alpha_{0c}$) is determined in the following paragraph.

The study of $\tilde{p}_1$ and $\tilde{p}_2$ variations versus $\alpha$ shows that there exists a particular value $\alpha^\star$ such that $\tilde{p}_1 = \tilde{p}_2$ at $\alpha = \alpha^\star$. In Fig. 2, they are labeled $\alpha_i^\star$ for $\alpha_0 = i$ with $i = 1$, 2, 3, and 4. When $0 < \alpha^\star < \pi$ or when $\alpha^\star \in$ Im (see $\alpha_1^\star$, $\alpha_2^\star$, and $\alpha_3^\star$ in Fig. 2), it is found that the buckled configuration evolves in a continuous and stable way with the pressure. When $\alpha^\star > \pi$ (see $\alpha_4^\star$ in Fig. 2), a shape instability or snap-through from upward to downward buckling may occur for the film. The critical value $\alpha_{0c}$ is then given by the following expression determined by finding $\alpha_0$, which verifies $\alpha^\star = \pi$:

$$\alpha_{0c} = \sqrt{\pi^2 + 2\frac{\pi^2 - 6}{\tilde{h}^2\pi^2}\tan^2\theta}. \tag{15}$$

In the cases in which $\alpha_0 > \alpha_{0c}$, it is found that the limits of $\tilde{p}_1$ and $\tilde{p}_2$ when $\alpha$ tends to $\pi$ are equal to $\tilde{p}_c$:

$$\tilde{p}_c = \lim_{\alpha\to\pi}\tilde{p}_1 = \lim_{\alpha\to\pi}\tilde{p}_2 = -\frac{\pi^2}{12}\tilde{h}^3\tan\theta. \tag{16}$$

To illustrate these statements, the profiles $\tilde{w}(\tilde{x} - \tilde{u}(\tilde{x}))$ versus $\tilde{x}$ have been plotted in Figs. 3(a), 3(c), and 3(e) for $\alpha_0 = 1$, 2, and 4, respectively, and for increasing pressure $\tilde{p}$ (in absolute value) from top to bottom profiles, which can alternatively be either $\tilde{p}_1$ or $\tilde{p}_2$, with $\tilde{h} = 0.1$ and $\theta = \pi/20$. For such values of the thickness and the folding angle, the critical value $\alpha_{0c}$ beyond which it has been suggested that the system is unstable is equal to 3.44. It is underlined that the pressure variation in Figs. 3(a), 3(c), and 3(e) corresponds to $\alpha$ variations with a step equal to 0.05 ($0.05i$, with $i^2 = -1$) for buckled configurations in compression (in tension). It is observed in Figs. 3(a) and 3(c) that for $\alpha_0 = 1$ and 2, respectively, the transition from upward to downward buckling is continuous. This evolution has been confirmed in Figs. 3(b), 3(d), and 3(f), where $\tilde{\delta}$ has been displayed versus $\tilde{p}$ for $\alpha_0 = 1$, 2, and 4, with $\tilde{h} = 0.1$ and $\theta = \pi/20$. Indeed, in Figs. 3(b) and 3(d), the $\tilde{\delta}$ evolution from A to B is observed to be continuous for $\alpha_0 = 1$ and 2 as the pressure increases (in absolute value) and $\tilde{\delta}$ continuously decreases to zero and then goes under the horizontal plane as the film buckles downward. The main difference between both cases lies in the stress state of the buckles with respect to pressure: for $\alpha_0 = 1$, the buckle is in tension at any pressure, whereas for $\alpha_0 = 2$, the buckle is in tension at low pressures, changes into compression at intermediate pressures, and goes back to tension at higher pressures.

For $\alpha_0 = 4$, Fig. 3(f) shows that, for pressures in the range $[\tilde{p}_l, \tilde{p}_r]$, three different configurations labeled A, B, and C are in equilibrium at the same pressure $\tilde{p}$. It is seen in Fig. 3(e) that A, B, and C correspond to upward, downward, and intermediate camel back buckle shapes, respectively. To study the stability of the three equilibria, the energy of the buckle configurations needs to be determined.

### B. Stability analysis of the equilibrium configurations

The total energy of the system is given by

$$E_{\text{tot}} = E_s + E_b - \tilde{p}\tilde{V}, \tag{17}$$

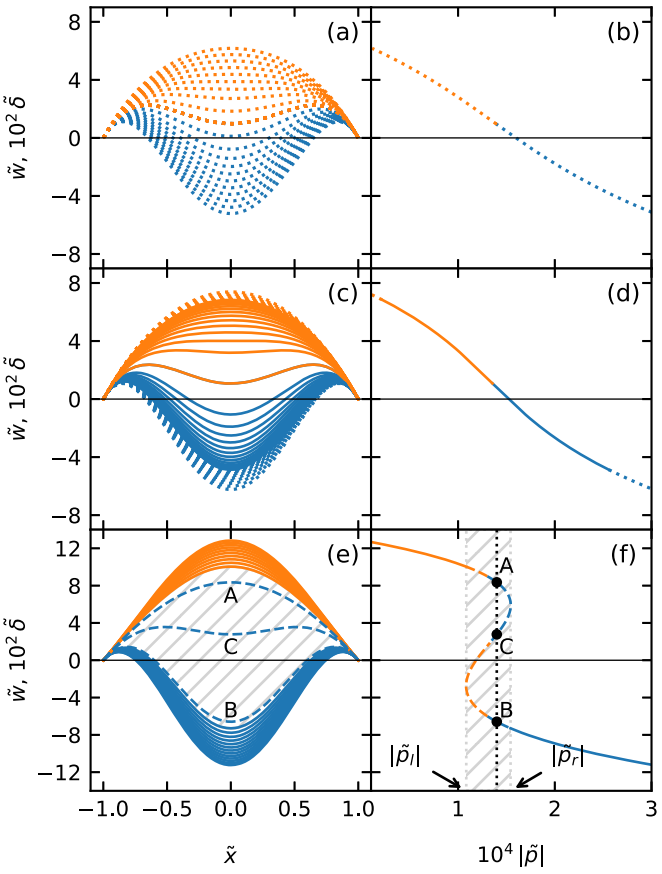


FIG. 3. Buckle evolution under pressure for $\theta = \pi/20$ and $\tilde{h} = 0.1$. Buckle profile $\tilde{w}(\tilde{x} - \tilde{u}(\tilde{x}))$ vs $\tilde{x}$ for (a), (c), (e) increasing pressure $\tilde{p}$ (from top profile to bottom) and (b), (d), (f) evolution of $\tilde{\delta}$ vs $\tilde{p}$ for (a), (b) $\alpha_0 = 1$; (c), (d) $\alpha_0 = 2$; and (e), (f) $\alpha_0 = 4$. Curves corresponding to pressures $\tilde{p}_1$ and $\tilde{p}_2$ (with $\tilde{p}_1 < \tilde{p}_2$) are, respectively, blue (dark gray) and orange (light gray). Solid lines are used for buckled configurations in compression, and dotted lines for those in tension. Dashed lines correspond to buckled configurations at pressures in the range $[\tilde{p}_l, \tilde{p}_r]$.

where the two terms $E_s$ and $E_b$ are the stretching and bending energies, respectively, written as [46]

$$E_s = \int_{-1}^{1} \frac{\tilde{h}}{2} \varepsilon_{xx}^2 d\tilde{x}, \tag{18}$$

$$E_b = \int_{-1}^{1} \frac{\tilde{h}^3}{24} \left( \frac{\partial^2 \tilde{w}}{\partial \tilde{x}^2} \right)^2 d\tilde{x}, \tag{19}$$

with $\tilde{u}$ and $\tilde{w}$ given by Eqs. (2) and (3), respectively, and the strain $\varepsilon_{xx}$ in the buckle is given by [13,46]

$$\varepsilon_{xx} = \varepsilon_0 + \frac{\partial \tilde{u}}{\partial \tilde{x}} + \frac{1}{2} \left( \frac{\partial \tilde{w}}{\partial \tilde{x}} \right)^2. \tag{20}$$

The third term in Eq. (17) represents the work of the pressure, with $\tilde{V}$ the volume below the buckle,

$$\tilde{V} = \int_{-1}^{1} \tilde{w}(\tilde{x} - \tilde{u}(x)) d\tilde{x} \approx \int_{-1}^{1} \tilde{w}(\tilde{x}) d\tilde{x}. \tag{21}$$

The evolution of the energy $E_{\text{tot}}$ has been calculated from configuration A to B, passing through C. To do so, a path

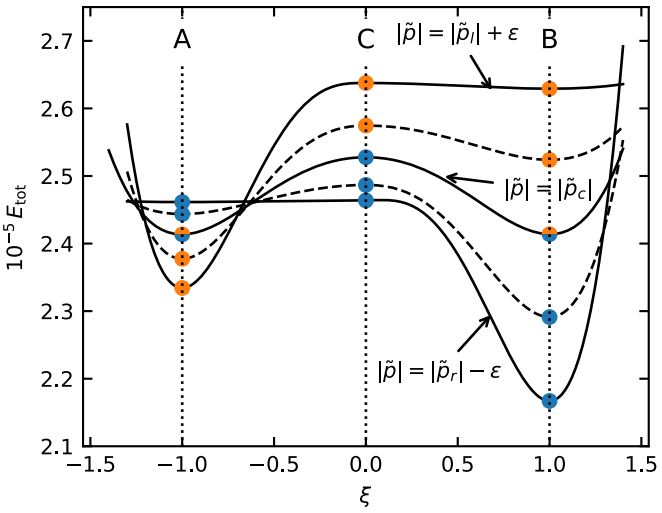


FIG. 4. Energy path between three buckle configurations A, B, and C in the range pressure $\tilde{p} \in ]\tilde{p}_l, \tilde{p}_r[$ for which the buckle can transit from the upward configuration A to the downward configuration B. The considered parameters are $\alpha_0 = 4$, $\theta = \pi/20$, and $\tilde{h} = 0.1$.

has been linearly interpolated between A, B, and C in the configuration space such that

$$\tilde{w}(x, \xi) = \begin{cases} -\xi \tilde{w}_A(x) + (1 + \xi)\tilde{w}_C(x) & \text{for } \xi \leqslant 0, \\ -\xi \tilde{w}_B(x) + (1 - \xi)\tilde{w}_C(x) & \text{for } \xi > 0, \end{cases} \tag{22}$$

and

$$\tilde{u}(x, \xi) = \begin{cases} -\xi \tilde{u}_A(x) + (1 + \xi)\tilde{u}_C(x) & \text{for } \xi \leqslant 0, \\ -\xi \tilde{u}_B(x) + (1 - \xi)\tilde{u}_C(x) & \text{for } \xi > 0, \end{cases} \tag{23}$$

where the configurations A, C, and B are found for $\xi = -1$, 0, and 1, respectively. Using $\tilde{u}(x, \xi)$ and $\tilde{w}(x, \xi)$ in Eqs. (18)–(21), $E_{\text{tot}}(\xi)$ has been calculated for any value $\xi \in [-1.2, 1.2]$ and plotted in Fig. 4 for some pressures $\tilde{p} \in ]\tilde{p}_l, \tilde{p}_r[$. It is seen that, for any pressure in the range $\tilde{p} \in ]\tilde{p}_l, \tilde{p}_r[$, configuration C is unstable (the energy is maximum) whereas configurations A and B are stable. It is recalled that A and B are the only stable configurations for $|\tilde{p}| < |\tilde{p}_l|$ and $|\tilde{p}| > |\tilde{p}_r|$, respectively. The energy of configuration A is lower than that of the B for $|\tilde{p}_l| < |\tilde{p}| < |\tilde{p}_c|$, and this is the opposite for $|\tilde{p}_c| < |\tilde{p}| < |\tilde{p}_r|$, the energies of both configurations being equal when $|\tilde{p}| = |\tilde{p}_c|$. This suggests a hysteresis behavior as described in Fig. 5. At low pressures $|\tilde{p}|$, configuration A is the most stable configuration, and $\tilde{\delta}$ continuously decreases as $|\tilde{p}|$ increases. At $\tilde{p} = \tilde{p}_c$, the energies of configurations A and B are equal and, as soon as $|\tilde{p}| > |\tilde{p}_c|$, configuration B has the lower energy and A becomes metastable. The system can remain in the metastable configuration A until the snap-through to B occurs at $\tilde{p} = \tilde{p}_r$, after which configuration B becomes the only stable configuration. The buckle is in configuration B and its maximum deflection $\tilde{\delta}$ continuously decreases as the pressure $|\tilde{p}|$ increases. From high pressure to low pressure, configuration B is first the most stable configuration, then it becomes metastable when $|\tilde{p}| < |\tilde{p}_c|$, and the snap-through from B to A finally occurs at $\tilde{p} = \tilde{p}_l$. Thus, the transitions from upward to downward buckling and from downward to forward buckling take place at two different pressures, exhibiting indeed a hysteresis behavior. It is worth noting

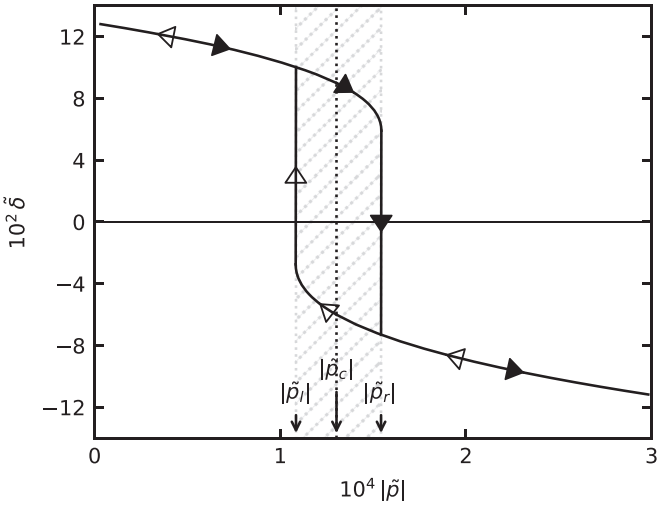


FIG. 5. Evolution of the maximum deflection $\tilde{\delta}$ with respect to the pressure $|\tilde{p}|$ for $\alpha_0 = 4$, $\theta = \pi/20$, and $\tilde{h} = 0.1$. The filled arrows correspond to the path from upward to downward buckling, and the empty arrows correspond to the path from downward to upward buckling.

that the two previously described regimes for the thin-film buckling, i.e., the continuous and discontinuous transitions, have also been observed (but not shown) while considering different folding angles $\theta$ at constant initial stress $\alpha_0 > \alpha_{0c}$ [Eq. (15)].

For convenience, the transition will be considered in the following to occur at the pressure $\tilde{p}_c$, i.e., when both upward and downward buckled configurations have the same energy.

## IV. STUDY OF THE BUCKLING BEHAVIOR WITH SUBSTRATE

The configuration where the film is delaminated on a length $2b$ after deposition on a continuous substrate has also been briefly addressed. Indeed, some information on the buckling state can be derived in this case from the freestanding analysis, considering the limit configuration where the snap-through or the continuous deposition leads to the situation in which the buckle amplitude is zero, i.e., $\delta = 0$, such that the buckled film touches the substrate under pressure. It is emphasized that the full redeposition process of the film and the contact modeling with the substrate are beyond the scope of the present analysis. Consequently, two other critical pressures $\tilde{p}_0$ and $\tilde{p}_c^0$ can be defined for the film touching the substrate. The pressure $\tilde{p}_0$ corresponds to the case in which $\tilde{\delta}$ goes to 0 without any abrupt transition as $\alpha \to 0$, i.e., when the film is fully released (without compression or tension). The other pressure $\tilde{p}_c^0$ is the pressure at which the buckle touches the substrate just after the abrupt transition, i.e., when $\alpha \to \pi$. It yields

$$\tilde{p}_0 = -\sqrt{\frac{35}{22}}\tilde{h}^4\alpha_0, \tag{24}$$

$$\tilde{p}_c^0 = -\frac{1}{3}\pi^2\tilde{h}^4\sqrt{\frac{\alpha_0^2 - \pi^2}{3\pi^2 - 16}}. \tag{25}$$

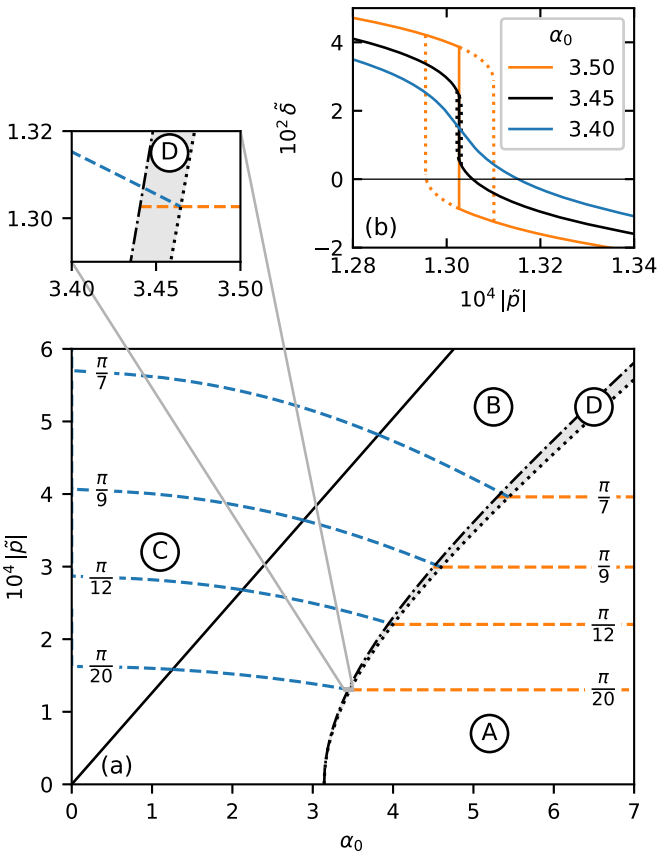


FIG. 6. (a) $(\alpha_0, |\tilde{p}|)$ diagram describing the thin-film behavior for $\tilde{h} = 0.1$. The straight black solid line is given by $|\tilde{p}_0|$ variation with respect to $\alpha_0$ [Eq. (24)] and delimits the region C (buckles in a tensile stress state) from the region B (buckles in a compressive stress state), the buckle touching the plane $z = 0$ by continuously increasing the pressure. The dash-dotted black curve, given by $|\tilde{p}_c|$ variation with respect to $\alpha_0$ [Eq. (26)], delimits the region B (continuous transition) from the regions D and A (abrupt upward to downward transition). The dotted black curve, given by $|\tilde{p}_c^0|$ variation with respect to $\alpha_0$ [Eq. (25)], delimits the region D, where the buckle touches the substrate after a snap-through for a pressure $|\tilde{p}| > |\tilde{p}_c|$, from the region A, where the buckle touches the substrate immediately after a snap-through at $|\tilde{p}| = |\tilde{p}_c|$. Dashed blue (dark gray) lines in the regions B, C, and D are the iso-$\theta$ curves indicating the pressure $\tilde{p}$ required for the buckles to touch the plane $z = 0$ ($\tilde{\delta} = 0$) vs $\alpha_0$. Dashed orange (light gray) lines give the critical pressure $|\tilde{p}_c|$ [Eq. (16)] at the abrupt transition in the regions A and D. (b) Evolution of $\tilde{\delta}$ with respect to $|\tilde{p}|$ for different values of the applied stress $\alpha_0 = 3.40$, 3.45, and 3.50. The hysteresis is displayed with dotted lines.

The critical pressure $\tilde{p}_c$ at which the snap-through phenomenon occurs can also be considered as a function of $\alpha_0$, without any consideration on the film position with respect to the substrate (contrary to $\tilde{p}_c^0$). Its expression is given by combining Eqs. (15) and (16):

$$\tilde{p}_c = -\frac{1}{12}\pi^3\tilde{h}^4\sqrt{\frac{\alpha_0^2 - \pi^2}{2\pi^2 - 12}}. \tag{26}$$

In Fig. 6(a), the thin-film behavior diagram, only valid in the case in which $\delta = 0$, has been displayed in the $(\alpha_0, |\tilde{p}|)$ plane for $\tilde{h} = 0.1$. The limits defined by Eqs. (24)–(26) split

the diagram into four regions A, B, C, and D. In region A, the deflection $\delta$ is equal to 0 as soon as the snap-through phenomenon from upward to downward buckling has taken place. In regions B and C, the transition is continuous, the buckle being in compression in region B and in tension in region C for any value of $\theta$ when the condition $\tilde{\delta} = 0$ is reached. From this configuration where $\delta$ is zero, the free-standing film can then go from the upper part of the plane to the lower part with increasing pressure, while in presence of a substrate the redeposition should take place. Region D defines a region where the buckle can undergo an abrupt transition at $\tilde{p} = \tilde{p}_c$ and can reach $\tilde{\delta} = 0$ at a pressure $|\tilde{p}| > |\tilde{p}_c|$. To highlight the differences between regions A, B, and D, the evolution of the deflection $\tilde{\delta}$ with respect to $|\tilde{p}|$ is plotted in Fig. 6(b) for $\tilde{h} = 0.1$, $\tan\theta = \pi/20$, and $\alpha_0 = 3.40$, 3.45, and 3.50 corresponding to regions B, D, and A displayed in Fig. 6(a), respectively. It can be seen that for $\alpha_0 = 3.40$, the buckle touches the substrate ($\tilde{\delta} = 0$) after $\tilde{\delta}$ has continuously decreased with increasing $|\tilde{p}|$, whereas it undergoes an abrupt upward to downward transition at $|\tilde{p}_c| \approx 1.30$ for $\alpha_0 = 3.45$ and 3.50. The contact between the buckle and the substrate occurs at $\tilde{p} = \tilde{p}_c$ for $\alpha_0 = 3.50$ and at $\tilde{p} > \tilde{p}_c$ for $\alpha_0 = 3.45$. It should be emphasized here that this analysis is valid only if the snap-through is assumed to occur at pressure $\tilde{p}_c$. In the case in which the hysteresis behavior is taken into account, the region D can disappear under certain conditions of applied stresses $\alpha_0$ and folding angles $\theta$, making the diagram much more difficult to read.

Solving together Eqs. (13) and (14) for $\tilde{\delta} = 0$, it is possible to plot, in regions B and C of the $(\alpha_0, |\tilde{p}|)$ diagram, iso-$\theta$ curves for which the position of the buckle center reaches $z = 0$. Other iso-$\theta$ curves corresponding to the abrupt transition at $\tilde{p} = \tilde{p}_c$ with respect to $\alpha_0$ [see Eq. (16)] have also been displayed in region A of Fig. 6. To sum up, the transition from upward to downward buckling can be described by following iso-$\theta$ curves in the $(\alpha_0, |\tilde{p}|)$ diagram. Taking $\theta = \frac{\pi}{20}$ as an example, it can be seen that the buckle can redeposit at $z = 0$ in a tensile stress state (region C) for $\alpha_0 < 1.25$ and in a compressive stress state (region B) for $\alpha_0 > 1.25$, the state at $\alpha_0 = 1.25$ corresponding to a completely released buckle. The pressure $|\tilde{p}|$ required to maintain $\tilde{\delta} = 0$ decreases from 1.61 to 1.30 as the applied stress $\alpha_0$ increases from 0 to 3.44. For $3.44 < \alpha_0 < 3.46$, the buckle configuration is found in region D (see the zoom in Fig. 6), where an abrupt transition occurs at $\tilde{p}_c \approx 1.30$, but $\tilde{\delta} = 0$ for a pressure $\tilde{p} > \tilde{p}_c$. Finally, for $\alpha_0 > 3.46$, the buckle configuration is found exclusively in region A where the transition from $\tilde{\delta} > 0$ to $\tilde{\delta} < 0$ occurs suddenly at $\tilde{p} = \tilde{p}_c$.

## V. CONCLUSION

The study of the buckling of a free-standing thin film clamped at its edges has been investigated in the framework of the Föppl–von Kármán theory of thin plates when the film is submitted to a compressive stress and to an applied pressure on its upper free-surface. Assuming that the film can undergo an upward folding at its edges due to the thin-film plasticity, including dislocations and/or grain boundaries, the buckling profile of the film has been determined and two different buckling regimes have been identified. Depending on the applied pressure and initial stress, the transition from upward to downward buckling can be either continuous or discontinuous. This transition (continuous or abrupt) has been theoretically characterized from a linear stability analysis as a function of the different parameters of the problem, such as the applied pressure, the compressive stress, and the folding angle, focusing on the conditions required for the buckle to snap from the upper to the lower plane. An hysteresis cycle for the thin-film buckling versus pressure has also been identified, and the strain state of the film (compression, tension) has been discussed. As such, these films could be considered for the design of nano-/microdevices such as sensors sensitive to pressure and stress. When the film is deposited on a continuous substrate and delaminated, the critical pressures for the redeposition onto the substrate (continuous or abrupt) have also been derived.

The next step of this work could be a study of the post-buckling regime and the dynamics of the snap-through. To do so, a numerical approach could be used to characterize this transition (continuous or abrupt) as a function of the different parameters of the problem identified in the present work, including the applied pressure, the compressive stress, and the folding angle. When the film is lying on a continuous substrate, its full redeposition should also be investigated numerically.

## ACKNOWLEDGMENTS

This work pertains to the French Government program "Investissements d'Avenir" (EUR INTREE, reference ANR-18-EURE-0010).

[1] N. Stoop, R. Lagrange, D. Terwagne, P. M. Reis, and J. Dunkel, Curvature-induced symmetry breaking determines elastic surface patterns, Nat. Mater. **14**, 337 (2015).

[2] J. Chopin and A. Kudrolli, Helicoids, Wrinkles, and Loops in Twisted Ribbons, Phys. Rev. Lett. **111**, 174302 (2013).

[3] F. Brau, P. Damman, H. Diamant, and T. A. Witten, Wrinkle to fold transition: influence of the substrate response, Soft Matter **9**, 8177 (2013).

[4] J. D. Paulsen, E. Hohlfeld, H. King, J. Huang, Z. Qiu, T. P. Russell, N. Menon, D. Vella, and B. Davidovitch, Curvature-induced stiffness and the spatial. variation of wavelength in wrinkled sheets, Proc. Natl. Acad. Sci. USA **113**, 1144 (2016).

[5] A. Morshedifard, M. Ruiz-García, M. J. Abdolhosseini Qomi, and A. Košmrlj, Buckling of thermalized elastic sheets, J. Mech. Phys. Solids **149**, 104296 (2021).

[6] S. Nagashima, H. D. Ha, D. H. Kim, A. Košmrlj, H. A. Stone, and M.-W. Moon, Spontaneous formation of aligned DNA nanowires by capillarity-induced skin folding, Proc. Natl. Acad. Sci. USA **114**, 6233 (2017).

[7] B. Roman and A. Pocheau, Postbuckling of bilaterally constrained rectangular thin plates, J. Mech. Phys. Solids **50**, 2379 (2002).

[8] S. Timoshenko and S. Woinowsky-Krieger, *Theory of Plates and Shells*, 2nd ed. (McGraw-Hill, New York, 1959).

[9] P. G. Ciarlet, *Mathematical Elasticity, Vol. III: Theory of Shells* (North Holland, Amsterdam, 2000).

[10] A. M. A. van der Heijden, *Koiter's Elastic Stability of Solids and Structures* (Cambridge University Press, New York, 2009).

[11] R. M. Jones, *Buckling of Bares, Plates and Shells* (Bull Ridge, Blacksburg, VA, 2006).

[12] A. Evans, M. Prestat, R. Tölke, M. V. F. Schlupp, L. J. Gauckler, Y. Safa, T. Hocker, J. Courbat, D. Briand, N. F. de Rooij, and D. Courty, Residual stress and buckling patterns of free-standing yttria-stabilized-zirconia membranes fabricated by pulsed laser deposition, Fuel Cells **12**, 614 (2012).

[13] J. Hutchinson and Z. Suo, *Mixed Mode Cracking in Layered Materials* (Elsevier, Amsterdam, 1991), pp. 63–191.

[14] L. B. Freund and S. Suresh, *Thin Film Materials: Stress, Defect Formation and Surface Evolution* (Cambridge University Press, Cambridge, 2004).

[15] K. Bertoldi, V. Vitelli, J. Christensen, and M. Van Hecke, Flexible mechanical metamaterials, Nat. Rev. Mater **2**, 17066 (2017).

[16] M. Kadic, G. W. Milton, M. van Hecke, and M. Wegener, 3D metamaterials, Nat. Rev. Phys. **1**, 198 (2019).

[17] C. Soukoulis and M. Wegener, Past achievements and future challenges in the development of three-dimensional photonic metamaterials, Nat. Photon. **5**, 523 (2011).

[18] J. U. Surjadi, L. Gao, H. Du, X. Li, X. Xiong, N. X. Fang, and Y. Lu, Mechanical metamaterials and their engineering applications, Adv. Eng. Mater. **21**, 1800864 (2019).

[19] S. Srivatsa, R. Suresh Kumar, D. Selva, and M. N. Silberstein, Examining the impact of asymmetry in lattice-based mechanical metamaterials, Mech. Mater. **172**, 104386 (2022).

[20] Y. Safa and T. Hocker, A validated energy approach for the post-buckling design of micro-fabricated thin film devices, Appl. Math. Modell. **39**, 483 (2015).

[21] M. Gomez, D. E. Moulton, and D. Vella, Critical slowing down in purely elastic 'snap-through' instabilities, Nat. Phys. **13**, 142 (2017).

[22] A. Fargette, S. Neukirch, and A. Antkowiak, Elastocapillary Snapping: Capillarity Induces Snap-Through Instabilities in Small Elastic Beams, Phys. Rev. Lett. **112**, 137802 (2014).

[23] A. Pandey, D. E. Moulton, D. Vella, and D. P. Holmes, Dynamics of snapping beams and jumping poppers, Europhys. Lett. **105**, 24001 (2014).

[24] M. Gomez, D. E. Moulton, and D. Vella, Passive Control of Viscous Flow via Elastic Snap-Through, Phys. Rev. Lett. **119**, 144502 (2017).

[25] F. Motazedian, Z. Wu, J. Zhang, B. S. Shariat, D. Jiang, M. Martyniuk, Y. Liu, and H. Yang, Determining intrinsic stress and strain state of fibre-textured thin films by X-ray diffraction measurements using combined asymmetrical and bragg-brentano configurations, Mater. Des. **181**, 108063 (2019).

[26] E. Chason, B. W. Sheldon, L. B. Freund, J. A. Floro, and S. J. Hearne, Origin of Compressive Residual Stress in Polycrystalline Thin Films, Phys. Rev. Lett. **88**, 156103 (2002).

[27] J. Hutchinson, M. Thouless, and E. Liniger, Growth and configurational stability of circular, buckling-driven film delaminations, Acta Metall. Mater. **40**, 295 (1992).

[28] G. Gioia and M. Ortiz, Delamination of compressed thin films, Adv. Appl. Mech. **33**, 119 (1997).

[29] B. Audoly, Stability of Straight Delamination Blisters, Phys. Rev. Lett. **83**, 4124 (1999).

[30] B. Audoly, B. Roman, and A. Pocheau, Secondary buckling patterns of a thin plate under in-plane compression, Eur. Phys. J. B **27**, 7 (2002).

[31] G. Parry, A. Cimetière, C. Coupeau, J. Colin, and J. Grilhé, Stability diagram of unilateral buckling patterns of strip-delaminated films, Phys. Rev. E **74**, 066601 (2006).

[32] S.-J. Yu, X. Xiao, M. Chen, H. Zhou, J. Chen, P. Si, and Z. Jiao, Morphological selections and dynamical evolutions of buckling patterns in $SiAlN_x$ films: from straight-sided to telephone cord or bubble structures, Acta Mater. **64**, 41 (2014).

[33] T. Guo, J. He, X. Pang, A. Volinsky, Y. Su, and L. Qiao, High temperature brittle film adhesion measured from annealing induced circular blisters, Acta Mater. **138**, 1 (2017).

[34] M. Cordill, F. Fisher, F. Rammerstorfer, and G. Dehm, Adhesion energies of Cr thin films on polyimide determined from buckling: experiment and model, Acta Mater. **58**, 5520 (2010).

[35] Y. Ni, S.-J. Yu, H. Jiang, and L. He, The shape of telephone cord blisters, Nat. Commun. **8**, 14138 (2017).

[36] M. Ortiz and G. Gioa, The morphology and folding patterns of buckling-driven thin film blisters, J. Mech. Phys. Solids **42**, 531 (1994).

[37] J. Colin, C. Coupeau, J. Durinck, and J. Grilhé, Buckling and cracking of $Y_2O_3$ thin films at grain boundaries, Phys. Rev. B **78**, 153411 (2008).

[38] J. Colin, C. Coupeau, and J. Grilhé, Plastic Folding of Buckling Structures, Phys. Rev. Lett. **99**, 046101 (2007).

[39] F. Foucher, C. Coupeau, J. Colin, A. Cimetière, and J. Grilhé, How Does Crystalline Substrate Plasticity Modify Thin Film Buckling? Phys. Rev. Lett. **97**, 096101 (2006).

[40] J. Li, Disclination model of high angle grain boundaries, Surf. Sci. **31**, 12 (1972).

[41] B. Bertin, J. Durinck, and J. Colin, Grain boundary-induced plasticity during thin film buckling, Mech. Mater. **155**, 103761 (2021).

[42] J. Colin, C. Coupeau, J. Durinck, A. Cimetière, and J. Grilhé, Redeposition of a straight-sided buckle under pressure, Phys. Rev. E **89**, 032410 (2014).

[43] S. Hamade, J. Durinck, G. Parry, C. Coupeau, A. Cimetière, J. Grilhé, and J. Colin, Effect of plasticity and atmospheric pressure on the formation of donut- and croissant-like buckles, Phys. Rev. E **91**, 012410 (2015).

[44] S.-J. Yu, G. Parry, C. Coupeau, and L. Li, Pressure-induced transition from wavy circular to ring-shaped buckles, Int. J. Solids Struct. **225**, 111053 (2021).

[45] S. Timoshenko and J. N. Goodier, *Theory of Elasticity* (McGraw-Hill, New York, 1952).

[46] L. Landau and E. Lifshitz, *Theory of Elasticity* (Pergamon, Oxford, 1970).